Available online at www.sciencedirect.com
SCIENCE DIRECT®
Polymer 44 (2003) 3607–3620
polymer
www.elsevier.com/locate/polymer

Molecular simulations of small gas diffusion and solubility in copolymers of styrene

Esra Kucukpinar[a,b], Pemra Doruker[a,*]

[a]*Department of Chemical Engineering and Polymer Research Center, Bogazici University, Bebek, Istanbul 34342, Turkey*
[b]*ARCELIK, Research and Technology Development Center, Tuzla, Istanbul 34950, Turkey*

Received 20 November 2002; received in revised form 10 February 2003; accepted 10 February 2003

Abstract

The objective of this study is to investigate the relationship between gas permeability and the chemical structure and conformational properties for copolymers of styrene and its homopolymer. The diffusion and the solubility coefficients of small gas molecules (He, H_2, Ne, O_2, N_2, CH_4, Ar, CO_2) in amorphous structures of poly (styrene-*alt*-maleic anhydride) copolymer (SMA), poly (styrene-*stat*-butadiene) rubber (SBR), and atactic polystyrene (PS) are investigated by the transition state approach. Simulation results are found to be in good agreement with the experimentally measured values. The transport behavior of H_2O molecules is also studied in the same bulk structures by fully atomistic molecular dynamics simulations. In general, the diffusion coefficients of the gases in these matrices decrease in the following order: SBR > PS > SMA, whereas the solubility coefficients follow the reverse order. The differences in the mobility of the matrices seem to be the dominant determining factor for diffusion. And the solubility coefficients depend on the free volume distribution of the matrices.

Keywords: Transition state approach; Poly(styrene-*alt*-maleic anhydride) copolymer; Styrene butadiene rubber

1. Introduction

The research on diffusion, sorption and permeation of small molecules in polymeric materials has always been fundamental, since there are many industrially important processes that utilize polymeric materials as membranes or barriers, such as food packaging, gas separation and encapsulation of electronic components [1,2]. In the last decade, it has become possible to establish structure–property relationships by means of molecular simulations [3], which would aid the design and material selection for the applications mentioned above.

Molecular dynamics (MD) simulation is an approach, which is effective for the investigation of the equilibrium and dynamic properties of polymeric microstructures. MD has been extensively used over the last 10 years in order to examine the diffusion mechanism of small gas molecules in polymers. The diffusion mechanisms of small molecules in polymer structures of poly(ethylene) [4,9], poly(propylene) [5,6], poly(isobutylene) [7–10], poly(dimethylsiloxane) [11–13], poly(butadiene) [14], poly(styrene) [15], poly-(imide) and poly(amide imide) [16,17], poly(vinyl alcohol) membranes [18], poly(vinyl alcohol) hydrogels [19], poly(benzoxazine) [20], poly(2,6-dimethyl-1,4-phenylene oxide) [21], poly[1-(trimethylsilyl)-1-propyne] [22], poly-(organophosphazenes) and poly(dibutoxyphosphazenes) [23], poly(ether-ether-ketone) [24] have already been investigated.

Transition-state approach (TSA) [25,26] is an alternative, efficient method that is commonly used to predict the diffusion coefficients and the solubility values, based on the transition-state theory. TSA is especially effective for polymeric systems with lower permeability coefficients, where MD simulations would not produce statistically reliable results due to computational time limitations [27–29].

In this work, the gas transport parameters, i.e. the diffusion coefficients and solubility values, for small penetrant molecules (He, H_2, N_2, Ne, O_2, CO_2, CH_4, Ar) in the amorphous structures of atactic polystyrene (PS), poly(styrene-*alt*-maleic anhydride) (SMA) and poly-(styrene-*stat*-butadiene) (SBR) are determined by means of TSA. In addition, the diffusion of water is studied in these

* Corresponding author. Fax: +90-212-2575032.
E-mail address: doruker@boun.edu.tr (P. Doruker).

0032-3861/03/$ - see front matter © 2003 Published by Elsevier Science Ltd.
doi:10.1016/S0032-3861(03)00166-6

matrices using fully atomistic MD simulations, which provide insight about the local structural relaxation and the free volume distributions of the matrices. Moreover, the specific interactions of the water molecules among themselves and with the matrices are investigated using pair correlation functions.

PS, a commodity polymer used in packaging, domestic electrical appliances, electronic equipments, and SBR, a copolymer of styrene widely used in products ranging from rubber bands to automotive tires, have both already been well-characterized experimentally. The experimental solubility, diffusion and permeability coefficients for most of the small penetrant molecules in PS and SBR are available. Another copolymer of styrene, SMA, used in auto parts and appliances, has been an active topic of research during recent years. To our knowledge, there have been no fully atomistic MD or TSA studies performed on SMA and SBR. Therefore our results will provide insight about the properties of SMA and SBR at the molecular level. There are several MD simulations performed on the PS matrix [15,30–32], but TSA results and the diffusion of H_2O in this matrix have not been reported so far. Although the three structures have the styrene monomer in common; PS (glass transition temperature, $T_g = 100$ °C) and SMA ($T_g = 170$ °C) are glassy, while SBR ($T_g = -20$ °C, when the weight percentage of styrene:butadiene is 50:50) [33] is rubbery at room temperature.

We would like to quantitatively compare these matrices with the aim of pinpointing those equilibrium and/or dynamic properties that play dominant roles in determining the differences among the gas transport parameters of these matrices. TSA will be particularly useful for the estimation of the diffusion coefficients of gases in the glassy systems due to its computational efficiency, whereas MD will provide more detailed information about the equilibrium and dynamic properties of these systems. As a result, the two copolymers containing styrene, SBR and SMA, will be characterized at a molecular scale, specifically in terms of gas transport properties.

2. Simulation details

2.1. Construction of polymer microstructures

Bulk structures of atactic polystyrene (PS), poly(styrene-*alt*-maleic anhydride) (SMA) and poly(styrene-*stat*-butadiene), also called styrene–butadiene rubber (SBR), were generated and simulated by using the commercial software of Accelrys (Insight II-Discover) [34]. The COMPASS (Condensed-phase Optimized Molecular Potentials for Atomistic Simulation Studies) forcefield was applied in all simulations [35]. The calculations were performed on SGI O_2 workstations.

Monomers and single chains. The structure of maleic anhyride monomer was built by the BUILDER module of InsightII [34]. The fundamental repeat units of styrene, maleic anhydride and *trans*-1,4 butadiene (*cis*-1,4 butadiene and 1,2-butadiene not shown) are given in Fig. 1(a)–(c), respectively. The potential types of the atoms for these repeat units (except hydrogen atoms) are also indicated in Fig. 1 according to the COMPASS Forcefield [35]. The structures of all monomers were initially subjected to energy minimization.

The general procedure used during all the energy minimization stages in this study starts with steepest-descent and changes to conjugate-gradient as the energy derivative on any atom decreases to 1000 kcal/mol. As this value reaches to 10 kcal/mol, it switches to Newton–Raphson, and then stops when it is below 0.001 kcal/mol or when at least 50,000 steps are completed.

After the energy minimization of monomers, single chains of required length and composition were formed by the POLYMERIZER module [34], and were subsequently subjected to energy minimization. The degree of polymerization values, DP, and the total number of atoms, N_{atom}, including H atoms, for the constructed chains are given in Table 1.

The homopolymer chains of PS were built using a mesodyad probability of 0.48. The chains of SMA and SBR were formed using the chirality inversion probability and probability of flip for the styrene monomer as 1.0 and 0, respectively. The repeat units of SMA chains (styrene and maleic anhydride) alternate along the chain, the weight percentage of styrene:maleic anhydride is 51.5:48.5.

SBR chains contain styrene (50% by weight), and three types of butadiene repeat units (50% by weight in total): (i) *trans*-1,4 (ii) *cis*-1,4 and (iii) 1,2 or vinyl butadiene. The statistical copolymer chains of SBR are formed by using the reactivity ratios of 0.8 and 1.4 for styrene and butadiene, respectively [36]. SBR-1 chain consists of 50% styrene, 35.5% *trans*-butadiene, 6.3% *cis*-butadiene, 8.2% 1,2

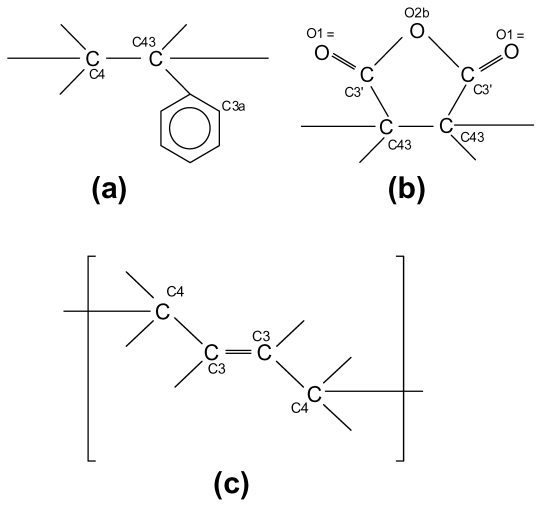

Fig. 1. The repeating units (a) styrene, (b) maleic anhydride, (c) *trans*-1,4 butadiene rubber with the COMPASS potential type assignments of atoms (the hydrogens are not explicitly shown).

Table 1
Details of the simulation systems

System	DP	N_{atom}	ρ_{exp} (g/cm^3)	ρ_{sim} [a] (g/cm^3)	Cell lengths[b] (Å)
PS-1	80	1282	1.04	1.024	23.82
PS-2	80	1282	1.04	1.040	23.67
SMA-1	140	1752	1.27	1.258	26.53
SMA-2	140	1752	1.27	1.256	26.55
SBR-1	120	1448	0.98	0.970	24.46
SBR-2	120	1448	0.98	0.950	24.65

[a] Equilibrium density of each system is calculated as an average over the final 30 ps of the equilibration NPT runs. Standard deviation varies in the range of 0.006–0.009.
[b] Calculated as an average over the final 30 ps of the equilibration NPT runs.

butadiene. SBR-2 chain has 50% styrene, 35.5% *trans*-butadiene, 5.0% *cis*-butadiene, 9.5% 1,2 butadiene.

Amorphous cell packing and annealing. The amorphous cells of the single chains were developed at 300 K by the AMORPHOUS_CELL module of InsightII [34]. In order to minimize chain end effects, each cell contains only one minimized polymer chain rather than several chains confined to the same volume, which would lead to increased density of chain ends. The amorphous cells are constructed using the method of Theodoreou and Suter [37]. In order to avoid generation of high energy configurations; the look-ahead feature of the AMORPHOUS_CELL module was used with a value of 5, with all 5 added at each step and the maximum number of look-ahead configurations was set to 50. The choice of states for PS was made according to the conventional interdependent RIS [38] model, while for the copolymer systems it was made automatically, according to the torsional potential for rotation about a given backbone bond.

Amorphous cells of PS, SMA and SBR were constructed at reduced densities of 0.85, 0.90 and 0.82 g/cm^3, respectively. The increased free volume at the lower density was sufficient for the generation of catenation-free structures. Following the cell construction at the initial density, NPT dynamics (DISCOVER, [34]) is performed at 0.5 GPa and 300 K to scale the cells to the specified experimental densities (ρ_{exp}), which are given in Table 1.

The cells were refined by the Basic_Refine Protocol of Insight II [34], which employs an initial energy minimization, a brief NVT run at 300 K and a final energy minimization. Later annealing was performed by NPT dynamics procedure at 1 bar using the Temperature Cycle Protocol of Insight II [34]. During annealing, the cells were first heated by 50 °C increments from 300 K to a temperature that is well above the glass transition temperature (T_g) of the polymer, chosen as 1000, 800 and 600 K for SMA, PS and SBR, respectively. Then the annealed cells were cooled back to 300 K using 50 °C increments. The duration of the NPT dynamics simulations at each temperature was 5000 fs.

Further equilibration. The annealed cells of the glassy polymers (SMA and PS) were later put through a stage-wise equilibration procedure. First each cell was pressurized at 300 K to increase its density well above the experimental one, and then the pressure was decreased in several stages to 1 bar. The aim was to obtain a refined system that would relax at the experimental density of the amorphous polymer at 1 bar and 300 K. Each stage consisted of three consecutive runs in the following order: (i) an NPT run at 300 K and a specific pressure, (ii) an NVT run at a high temperature well above T_g (800 K for PS and 1000 K for SMA), and (iii) an NVT run at 300 K. The pressures of the NPT run (step i) at different stages were sequentially set at $P = 0.5$, 3.0, 1.0 and 0.5 GPa. Each of the three consecutive runs in all stages was applied for 50,000 fs in SMA-1, SMA-2 and PS-1. In PS-2 cell, shorter runs of 25,000 fs were used instead.

In the case of rubbery SBR, each annealed cell was briefly compressed at 1 GPa for 5000 fs, followed by NVT at 300 K for 50,000 fs.

Finally, all systems, whether rubbery or glassy, were relaxed by NPT dynamics at 1 bar and 300 K to ensure that a constant density has been reached. This final equilibration step is carried out for 85,000–110,000 fs in the case of glassy polymers and for more than 200,000 fs in SBR. The average cell densities and the equilibrium cell lengths using the last 30 ps of the final NPT run are given in Table 1. The error between the experimental and the average predicted densities of the equilibrated cells are 1.54, 0, 0.95, 1.1, 1.02, and 3.1% for PS-1, PS-2, SMA-1, SMA-2, SBR-1 and SBR-2, respectively.

In all runs, Andersen method was used for temperature control [39]. In NPT runs, the pressure was controlled by Berendsen's method, where 0.1 ps and 0.5 GPa^{-1} were used as the pressure scaling constant (τ) and system compressibility value (β), respectively [40]. During these simulations, the cutoff for the nonbonded interactions was taken as 11.5 Å for PS, 13 Å for SMA and 12 Å for SBR. The spline and buffer widths were 2 and 1.5 Å. And the time step was 1 fs.

2.2. MD simulation of water diffusion

Diffusion coefficients of H_2O molecules in the equilibrated cells of PS-2, SMA-1 and SBR-1 were determined by NVT dynamics at 300 K.

For this aim, five H_2O molecules were inserted into the equilibrated PS and SBR microstructures, whereas eight H_2O molecules were used for SMA. The water molecules were positioned at the free volume sites of the cells such that the distance between any pair of H_2O was at least 8 Å for PS, 9 Å for SMA and 10 Å for SBR. After insertion of water molecules, the systems were subjected to energy minimization first by fixing the polymer atoms and afterwards by setting them again free. For the SMA and SBR cells, after an NVT dynamics of 105,000 fs, the systems were relaxed by NPT dynamics at 1 bar for 1500 fs. The resulting densities

of PS, SMA and SBR cells including the H_2O molecules were 1.05, 1.27, 0.97 g/cm^3, respectively. These cells were later subject to NVT dynamics for 2 ns (Discover_3). The data collection started after 75,000 fs for PS and after 60,000 fs for SMA and SBR.

In these calculations, the velocity Verlet algorithm was used with a time step of 1 fs. Andersen temperature control was used with the same parameters. The cut-off for non-bonded interactions was set to 11 Å, using respective spline and buffer widths of 2 and 1.5 Å.

From the trajectories recorded at 1 ps intervals, the consecutive positions of the water molecules diffusing in the polymer matrix are computed as a function of time. The diffusion coefficients of the water molecules can be calculated by means of the Einstein relation

$$D = \frac{\langle r^2 \rangle}{6t}, \quad t \to \infty \tag{1}$$

Here $\langle r^2 \rangle = \langle |\boldsymbol{r}(t) - \boldsymbol{r}(0)|^2 \rangle$ is the mean square displacement (MSD) of the penetrants over time, t. The brackets show that the average was taken for all the penetrant molecules over all time origins.

2.3. Diffusion and solubility of small gases by TSA

TSA [25,26] is used to compute the solubility values and diffusion coefficients for various kinds of gases in amorphous polymer microstructures. The COMPASS forcefield and the programs gsdif and gsnet are used for all the TSA calculations [41]. The Lennard–Jones parameters, σ_i and ε_i, used for the united atom representations of COMPASS forcefield are given in Table 2 for eight different penetrant molecules.

The method assumes that gases diffuse through dense polymer systems by a series of activated hops, which are independent from the structural relaxation of the polymer matrix and depend only on the elastic motion of the matrix [27]. This assumption is only valid for the diffusion of small molecules (not larger than methane) through the polymers. The isotropic elastic motion of the matrix is characterized by a smearing factor, $\langle \Delta^2 \rangle$, which represents the fluctuations (MSD) of the polymer atoms around their equilibrium positions. An identical $\langle \Delta^2 \rangle$ is used for all the atoms in the matrix.

Table 2
Lennard–Jones parameters used for the penetrant molecule interactions in TSA [41]

Penetrant	σ_i (Å)	ε_i (kcal/mol)
He	2.90	0.0203
H_2	2.93	0.0735
Ne	3.13	0.0709
O_2	3.46	0.2344
N_2	3.70	0.1889
CH_4	3.82	0.2945
Ar	3.84 (3.65)[a]	0.2464
CO_2	4.00 (3.70)[a]	0.4500

[a] The data in parentheses are modified according to the correlation presented in Fig. 2.

An amorphous cell (equilibrated by the methods described in Section 2.1) is transformed into an orthogonal lattice with a constant spacing of 0.3 Å. The solute distribution function in the matrix, $\rho(\mathbf{r})$, is evaluated by calculating the Helmholtz free energy between a gas molecule inserted at each grid point and all the atoms of the polymer matrix that are subject to elastic fluctuations. As a result, the local maxima in $\rho(\mathbf{r})$ are identified as different free volume sites in the matrix. The rate constants and the probabilities for the penetrant jumps from one free volume site to another are then determined together with the residence times in each site.

In this study, the smearing factor, $\langle \Delta^2 \rangle$, is computed using the self-consistent field procedure (SCF, auto-smearing) option of gsnet [41]. The MSD of all polymer atoms is obtained as a function of time from a short NVT dynamics (20 ps) without penetrant molecules. In SCF procedure, an initial guess is made for $\langle \Delta^2 \rangle$ in order to calculate the distribution of the penetrant residence times in the free volume sites. The most probable residence time is used to determine the MSD of atoms from the NVT dynamics results, hence the new $\langle \Delta^2 \rangle$. The same process is repeated until a convergence of $\langle \Delta^2 \rangle$ values is obtained.

Once the smearing factor and the corresponding jump probabilities are determined, the trajectories of the penetrant molecules are calculated by a Monte Carlo (MC) type procedure. The diffusion coefficient is then obtained by using Eq. (1), as an average over 1000 independent MC trajectories.

For low pressures ($p \ll 1$), the solubility, S, can be computed by using the TSA [27],

$$S = \frac{1}{kTV} \int \rho(\mathbf{r}) \mathrm{d}V \tag{2}$$

Here k represents the Boltzmann's constant and T is the temperature. The integral over the volume of the amorphous cell is actually a summation over all the lattice sites.

Once the diffusion and solubility values are computed, the permeability, P values can be calculated by the relation (3)

$$P = DS \tag{3}$$

3. Results and discussion

3.1. Evaluation of the TSA results

Table 3 lists the smearing factors calculated by the self-consistent field procedure for all types of penetrant molecules in each cell. These values fall in the same range with the smear factors used by Gusev et al. for glassy

Table 3
The smearing factors $\langle \Delta^2 \rangle^{1/2}$ (Å) calculated for the different gases in each matrix

Gas matrix	He	H_2	Ne	O_2	N_2	CH_4	Ar	CO_2
SBR-1	0.49	0.46	0.56	0.60	0.58	0.55	0.60	0.61
SBR-2	0.48	0.46	0.54	0.57	0.56	0.54	0.58	0.61
PS-1	0.44	0.42	0.51	0.55	0.54	0.51	0.55	0.56
PS-2	0.40	0.38	0.44	0.46	0.46	0.45	0.47	0.47
SMA-1	0.37	0.35	0.40	0.42	0.42	0.42	0.42	0.42
SMA-2	0.37	0.34	0.40	0.40	0.42	0.40	0.42	0.43

atactic polyvinylchloride and rubbery polydimethylsiloxane structures [27].

Table 4 gives the computed densities of the specific snapshots, chosen for TSA calculations. The free volume percentages and solubility parameters, $\delta_{(sim)}$, of these cells are also listed together with experimental solubility parameters, $\delta_{(exp)}$.

Diffusion. The diffusion coefficients, D_{sim}, calculated by TSA at 300 K for various gases, are compared with the available experimental data (D_{exp}) for PS [15,42–44] and SBR [33] in Table 5. We could not find any experimental diffusion coefficients for SMA in literature. In the case of SBR, experimental results are for statistical copolymers with butadiene/styrene content of 77:23 (wt:wt parts%), whereas the SBR composition in our simulations is 50:50. In general, there is very good agreement between experimental and simulation results for the relatively smaller gases. For the comparatively larger gases, Ar and CO_2, the diffusion coefficients are underestimated by more than one order of magnitude. In the following, we will show that these errors could be minimized by small adjustments of the σ parameters.

Teplyakov and coworkers have developed the following correlation based on extensive experimental data with different gases and polymer matrices [45]

$$\log D = K_1 - K_2 d_{\text{eff}}^2 \tag{4}$$

Here, d_{eff} is the effective penetrant diameter. The correlation coefficients K_1 and K_2 depend on the chemical and physical properties of the polymer matrices. This correlation holds for both glassy and rubbery polymers, as well as for homopolymers and copolymers.

Fig. 2 shows the correlation between d_{eff} values adopted by Teplyakov and Meares [45] and the σ values used in TSA calculations in Table 2. In this figure, the empty diamonds denote the original σ values assigned to each gas. The original σ values for Ar and CO_2 seem to be slightly higher than those depicted by d_{eff}. After a modification of these σ values, which are indicated in parentheses in Table 2 and by the filled diamonds in Fig. 2, the correlation coefficient increased from 0.94 to 0.98. More importantly, D_{sim} for Ar and CO_2 (given in parentheses in Table 5) are now closer to D_{exp} within acceptable limits.

In TSA calculations, the linear gases, i.e. O_2, N_2 and CO_2, are also represented as spherically symmetric molecules. For these gases, the effective σ parameter used in the Lennard Jones potential would be highly weighted towards the longest axis of the linear molecule, resulting in an overestimation of the minimal cross-sectional area of the molecule. Consequently, the diffusion coefficient, being more sensitive to the minimal cross-sectional area, might be underestimated in TSA, specifically in the case of CO_2.

In Fig. 3, the logarithms of D_{exp} (at 298 K) and D_{sim} (at 300 K) are plotted as a function of d_{eff}^2 to check if the correlation holds for our amorphous systems. For a clearer representation, the diffusion coefficients for Ar and CO_2 are those calculated with modified σ parameters, i.e. the values given in parenthesis in Table 5. The open circles, squares and triangles give the computed diffusion coefficient (D_{sim}) values, averaged over the two cells of SMA, PS and SBR, respectively. The lines represent the least squares fit through average D_{sim} values for each matrix with R^2 values of 0.98 in all cases.

D_{exp} are also shown on the same plot for PS (filled

Table 4
Properties of the specific cells chosen for TSA calculations

System	ρ[a] (g/cm^3)	Free volume%[b]	Solubility $\delta_{(exp)}$ (MPa)$^{1/2}$	Parameters $\delta_{(sim)}$ (MPa)$^{1/2}$
SBR-1	0.974	4.9	17.5–17.8[c]	14.9
SBR-2	0.957	7.2		15.9
PS-1	1.026	10.1	17.5–18.7[d]	13.4
PS-2	1.029	10.2		12.5
SMA-1	1.268	7.7	16.2–19.7[e]	16.4
SMA-2	1.251	12.8		8.2

[a] Density of the specific cell used for TSA.
[b] Free volume% = (V_f/total volume of the amorphous cell) × 100.
[c] Experimental data for butadiene/styrene 60:40 [36].
[d] Experimental data from Ref. [36].
[e] The value is obtained by three different group contribution methods [36].

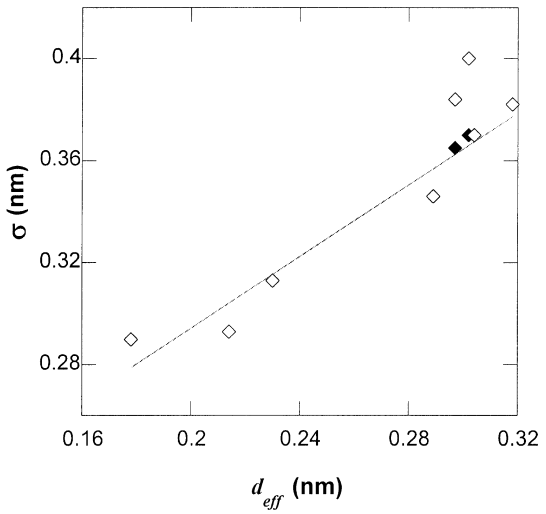

Fig. 2. Correlation between the effective penetrant diameter (d_{eff}) from Ref. [45] and Lennard Jones parameters (σ_i) used in TSA calculations. The solid diamonds represent modified (σ_i) values for CO_2 and Ar.

Table 5
Experimental (D_{exp}) and simulated (D_{sim}) diffusion coefficients (cm^2/s) for SBR, PS and SMA

Gas type	Cells	$D_{exp} \times 10^8$ (SBR)	$D_{sim} \times 10^8$ (SBR)	$D_{exp} \times 10^8$ (PS)	$D_{sim} \times 10^8$ (PS)	$D_{sim} \times 10^8$ (SMA)
He	Cell-1	–	2600	1040[a]	1400	680
	Cell-2		2100		1500	680
H_2	Cell-1	900[b]	1400	436[a]	510	170
	Cell-2		1000		600	170
Ne	Cell-1	–	620	240[c]	210	50
	Cell-2		340		160	50
O_2	Cell-1	140[b]	160	11[a]	24	1.2
	Cell-2		39		8.0	1.2
N_2	Cell-1	100[b]	90	6[d]	6.1	0.2
	Cell-2		13		2.1	0.3
CH_4	Cell-1	–	39	1.6[e]	1.2	0.03
	Cell-2		3.7		0.4	0.03
Ar	Cell-1	–	51 (86)[f]	24[c]	2.0 (7.3)[f]	0.03 (0.2)[f]
	Cell-2		4.7 (17)[f]		0.5 (2.1)[f]	0.04 (0.3)[f]
CO_2	Cell-1	105[b]	18 (40)[f]	5.8[a]	0.3 (3.3)[f]	0.0006 (0.03)[f]
	Cell-2		1.3 (7.3)[f]		0.03 (0.6)[f]	0.002 (0.06)[f]

[a] Ref. [42].
[b] Ref. [33]. Butadiene/styrene (wt:wt parts%) 77:23.
[c] Ref. [43]. The values are read from a figure.
[d] Ref. [44].
[e] Ref. [15].
[f] The values for the two gasses (Ar and CO_2) that are given in parentheses are computed by the σ_{Ar} and σ_{CO_2} of Table 2 shown in parentheses.

squares) [12,15] and for SBR (filled triangles) [33]. In general, there is good agreement between experimental and computed diffusion coefficients. For PS, the factor D_{sim}/D_{exp} changes between 0.6–1.5, except for the larger gases Ar ($D_{sim}/D_{exp} = 0.2$) and CO_2 ($D_{sim}/D_{exp} = 0.3$). For SBR, this factor is found to lie in almost the same range. However, the styrene content of SBR used in our simulations is higher than that reported in the experiments, which can be a reason for the underestimation in the case of larger gases. In summary, all of our systems, whether glassy or rubbery, conform to Eq. (4).

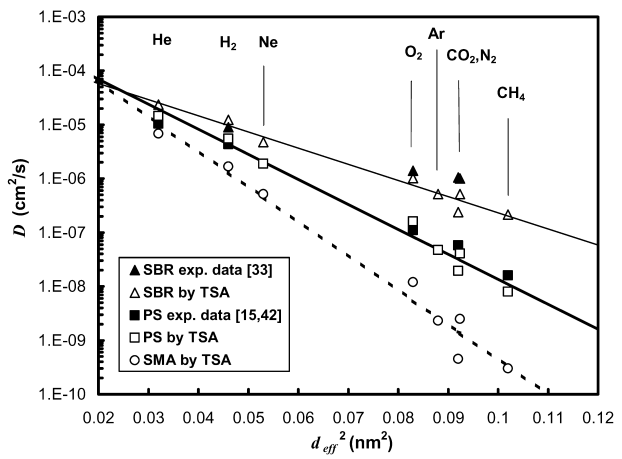

Fig. 3. Experimental and computed diffusion coefficients as a function of the squared effective penetrant diameter (d_{eff}^2) for SBR, PS and SMA systems. The lines are drawn through the TSA results according to Eq. (4).

The correlation coefficients K_1 and K_2 are given in Table 6 for both experimental and computed data. K_1 is much less sensitive to the polymer properties than K_2, as also indicated by Teplyakov and Meares [45]. Our results show that K_2 (SMA) > K_2(PS) > K_2(SBR), which follows the general trend proposed as: K_2 (glassy polymers with polar side groups) > K_2 (glassy polymers with nonpolar side groups) > K_2 (rubbery polymers) [45]. In these polymeric systems that possess quite different K_2 parameters, the differences between the diffusion coefficients of the

Table 6
Correlation coefficients evaluated for Eqs. (4) and (5)

Polymer	Styrene (wt%)	Method	K_1	K_2	K_3	$K_4 \times 10^2$
SBR	8	Exp.[a]	−4.24	18.4	−7.05	0.72
SBR	23	Exp.[b]	−4.11	20.6	−6.89	0.79
SBR	40	Exp.[a]	−4.00	25.3	−7.28	0.85
SBR	50	TSA	−3.64	30.0	−6.67	0.89
PS	100	Exp.[c]	−3.54	41.7	−6.73	1.04
PS	100	TSA	−3.23	46.4	−6.36	0.94
SMA	50	TSA	−2.94	64.2	−6.44	1.30

[a] Correlation coefficients from Ref. [45].
[b] Coefficients found by curve fitting through the experimental data from Ref. [33].
[c] K_1, K_2 found by curve fitting through the data from Ref. [42], and K_3, K_4 from Ref. [47].

structures increase as the effective penetrant diameter increases.

Moreover, the K_1 and K_2 parameters increase as the styrene content in the SBR increases and our simulation is also very consistent with this trend. In fact, our TSA results for SBR compares much more closely with the correlation provided for butadiene/styrene 60:40 [45], which is clear from the K_1 and K_2 parameters in Table 6.

At first glance, the K_2 values for our systems seem to increase as the glass transition temperature increases. This effect is related to the local mobility of the matrices represented by the smearing factors in TSA (see Table 3). For example, increasing the smearing factors for O_2 in SMA-1 and SMA-2 to the value for PS-1, resulted in comparable diffusion coefficients for SMA and PS. The D_{sim} of O_2 in SMA increased to 21×10^{-8} cm^2/s. However, the D_{sim} of O_2 in the rubbery matrix decreased (from 160×10^{-8} to 93×10^{-8}) but not to the levels of diffusion in PS, when the smearing factor of PS-1 is adopted for SBR-1.

However, the glass transition temperature cannot be the only determining factor. For example, poly(phenylene oxide) with a higher T_g (220 °C) than SMA has a K_2 value of 37.3 [45] and a much higher diffusion coefficient than expected [21,46]. As a result of numerous experimental data, Teplyakov and Meares [45] have indicated that K_2 increases as the cohesive energy density (CED) of the polymer matrices increase. Hence, we report the solubility parameters (δ) for our matrices, defined as $\delta = (\Delta E/V)^{1/2}$, where ΔE is the cohesive energy and V is the molar volume. The solubility parameters of the specific snapshots chosen for TSA are given in Table 4, together with the experimental ranges obtained from literature. The reported range for SMA is determined by using three different group contribution methods [36]. Looking at the solubility parameters obtained from literature, we cannot detect appreciable differences between the three matrices in order to draw conclusions about the relationship between cohesive energy density and diffusion. Comparison of simulation results (averaged over two cells) with the δ values from literature indicates errors in the ranges of 26–31% for PS, 24–38% for SMA and 12–13% for SBR. In general, the solubility parameters of our cells are underestimated, with the errors being higher for the glassy matrices, which represent non-equilibrium, frozen states. Specifically, SMA-2 has a very low δ value compared to SMA-1 with a closer δ value to the group contribution predictions. However, we cannot observe a significant difference between the diffusion coefficients of these two SMA cells that have very different CEDs.

In general, the diffusion coefficient estimates from TSA seem to be quite good (much closer than one order of magnitude to the experimental values) for all the penetrants considered. So far, the smear factors of the matrices, i.e. the local mobility, seem to be the dominant factor for the differences in the diffusion values obtained by TSA. In what follows, we would like to analyze the differences in free volume distributions of the matrices and their possible effects on gas transport properties.

Free volume distributions. The free volume calculations were done by the transition state approach of Gusev and Suter [25–27]. As explained before, the amorphous cell is divided into equally spaced lattice sites. Then, each lattice site is assigned either as an unoccupied or an occupied site by the polymer chain depending on the Helmholtz free energy between the probe molecule (helium) located at this site and the polymer matrix. A steepest-descent gradient path is started from each unoccupied grid point, which would terminate at a local minimum of the Helmholtz free energy. Thus, the collection of grid points belonging to each local minimum determines a specific free volume site and its corresponding volume, V_i. The free volume distribution in each cell, i.e. the number of the free volume sites (N_i) having a certain size (V_i) is determined. As a result, the total free volume of the cell is calculated as $V_f = \sum N_i \times V_i$. The accessible free volume (V_a) is defined as the summation of the free volumes of those sites having sizes equal or greater than a threshold volume (V_t), which would allow the diffusion of a specific penetrant with volume V_t, i.e. $V_a = \sum N_i \times V_i$, for $V_i \geq V_t$. The accessible free volume fraction (f_a) is given as [23]

$$f_a = \frac{V_a}{V_f} \tag{5}$$

In Fig. 4, the accessible free volume fraction is plotted as a function of the threshold free volume size for each cell. As expected, f_a decreases as the threshold value or the diffusing penetrant size (V_t) increases in all cells. The glassy structures of PS and SMA have higher accessible free volume contents than rubbery SBR. This is also related to the underestimation of the CED values in glassy matrices, discussed in the preceeding section on diffusion. The total free volume percentage of each cell is listed in Table 4

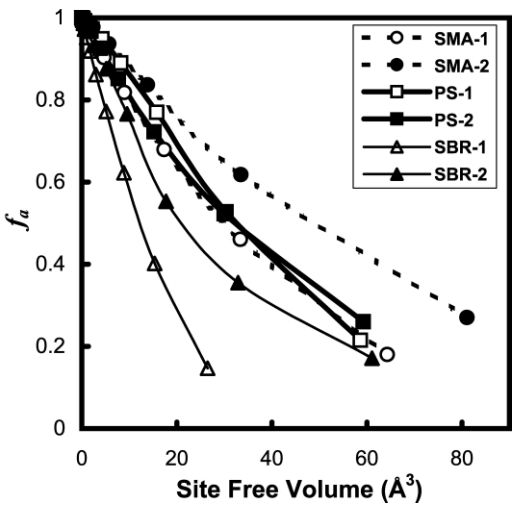

Fig. 4. Accessible free volume fraction, f_a, as a function of site free volume for each cell (refer to Eq. (5)).

taking He as the probe molecule. Again, SMA-2 with the highest free volume content has the lowest CED among all the matrices, which reflects the fact that it is highly unrelaxed. Yet, the diffusion coefficients in SMA-2 are almost the same as SMA-1, which has a much lower free volume percentage. Thus, the free volume content of the matrices is not a distinguishing factor for the observed differences in diffusion coefficients among the different matrices. In Section 3.2, we will also consider possible correlation between free volume distributions and solubility values.

Solubility. Table 7 lists the experimental (S_{exp}) [33,47] and computed (S_{sim}) solubility values for the polymeric systems. In general, S_{sim} values are higher than the experimentally measured values by a factor ranging between 1.5–2.7 for PS and 1.6–3.0 for SBR (no values reported for SMA). Similar differences between experimental and computed solubility values have been observed in previous TSA studies, as well [27,28].

Solubility of gases in a specific polymer matrix increases as the effective value of the Lennard–Jones potential-well depth (ε/k) of the gas increases (listed in Table 2). The logarithms of S_{sim} values for various gases are plotted in Fig. 5 as a function of (ε/k) of each penetrant, according to the correlation [45]

$$\log S = K_3 + K_4(\varepsilon/k) \quad (6)$$

S_{sim} values in Fig. 5 are the averages of the solubility values for the two equilibrated cells of each matrix. Again the lines representing the least squares fit through the S_{sim} values (with $R^2 = 0.99$, 0.97, 0.99 for SMA, PS and SBR, respectively) are drawn and the correlation coefficients, K_3 and K_4, are listed in Table 6. The K_3 values of these matrices do not differ too much, while K_4 values slowly increase in the order: $K_4(\text{SMA}) > K_4(\text{PS}) > K_4(\text{SBR})$. The compilation of Teplyakov and Meares has shown that K_4 for different polymers varies in the range of 0.72 and 1.47, with the polar matrices having higher values [45]. Our TSA results are in conformity with this trend.

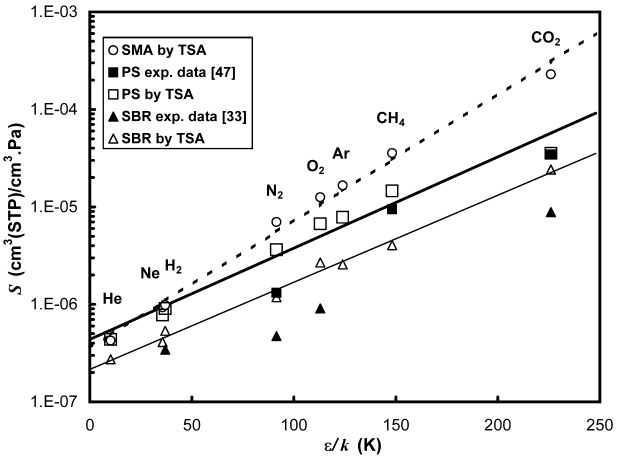

Fig. 5. Experimental and computed solubility values as a function of the penetrant Lennard–Jones potential well depth (ε/k) for SMA, PS and SBR systems. The lines are drawn through the TSA results according to Eq. (6).

Even though S_{exp} are not available for SMA structure, Eq. (6) provides a good fit for S_{sim} values of the copolymer structure. The S_{sim} values for SMA are significantly higher than the values for PS, especially for the gases with higher Lennard–Jones potential-well depth. In summary, our

Table 7
Experimental (S_{exp}) and simulated (S_{sim}) solubility values for SBR, PS and SMA (S is in cm^3(STP)/cm^3 Pa)

Gas type	Cells	$S_{exp} \times 10^8$ (SBR)	$S_{sim} \times 10^8$ (SBR)	$S_{exp} \times 10^8$ (PS)	$S_{sim} \times 10^8$ (PS)	$S_{sim} \times 10^8$ (SMA)
He	Cell-1	–	21	–	43	34
	Cell-2		33		44	51
H_2	Cell-1	34.2[a]	40.	–	89	77
	Cell-2		67		92	120
Ne	Cell-1	–	28	–	73	73
	Cell-2		54		82	110
O_2	Cell-1	91.1[a]	150	–	570	970
	Cell-2		390		770	1500
N_2	Cell-1	47.3[a]	53	131.2[b]	290	540
	Cell-2		180		430	860
CH_4	Cell-1	–	150	946.7[b]	1100	2800
	Cell-2		660		1800	4300
Ar	Cell-1	–	70 (120)[c]	–	520 (630)[c]	1400 (1300)[c]
	Cell-2		320 (390)[c]		870 (930)[c]	2000 (2000)[c]
CO_2	Cell-1	885.7[a]	400 (1100)[c]	3453.2[b]	4600 (6200)[c]	26000 (19000)[c]
	Cell-2		2500 (3700)[c]		9800 (9800)[c]	30000 (27000)[c]

[a] Ref. [33]. Butadiene/styrene (wt:wt parts%) 77:23.
[b] The S_{exp} of the three gases (CO_2, CH_4, N_2) in PS are the values for very low pressures from Ref. [47].
[c] The values for the two gasses (Ar and CO_2) that are given in parentheses are computed by the σ_{Ar} and σ_{CO_2} of Table 2 shown in parentheses.

TSA results at low pressures indicate the following trend: $S(SMA) > S(PS) > S(SBR)$.

The free volume distributions of the matrices emerge as a factor that affects the solubility of gases (see Fig. 5). Comparison of the two different cells of SMA indicate that SMA-2 with the higher free volume content and distribution leads to higher gas solubilities. Similar results are obtained for SBR. The average free volume distribution of two cells in each matrix (not shown) decreases in the following order: SMA > PS > SBR.

Simulations on glassy polystyrene matrices have shown that solubilities of larger gases (CO_2 and CH_4) are affected by the periodic system size chosen [30]. Specifically, the larger cavities that can accommodate these gases are formed in larger boxes and as a result the solubility predictions are closer to experimental values. Another simulation study on glassy polypropylene cells with various sizes has indicated significant system size effect on the solubility of larger gases, but no effect on the diffusive behavior of penetrants [6]. These results on glassy polymers are in conformity with our TSA results, which designate that the free volume distributions affect the solubility values but not the diffusion coefficients. Moreover, our simulation sizes seem proper for the estimation of diffusion coefficients, but may be not large enough for the estimation of the solubility parameter of the larger gases (CO_2 and CH_4), in view of these previous studies [6,30].

Permeability. Table 8 compares the experimental and simulated permeability coefficients for the three matrices. In general, the computed values are higher than experimental ones, which mainly result from the overestimations of solubility. Only in SBR, the permeability for the larger gases (N_2, CH_4, Ar and CO_2) is underestimated due to the lower predictions of diffusion. Again we should mention that the reported experimental values for SBR are obtained from a sample with a higher butadiene (77%) content than our simulations (50%), which would mean that $D_{exp} > D_{sim}$.

The only experimental data that we could obtain for SMA are permeability coefficients for O_2 and CO_2 in a sample containing 25 wt% maleic anhydride. Our predictions seem to fall into a reasonable range of these data, which indicates that TSA result on diffusion and solubility of the SMA matrix should be reliable, i.e. within an order of magnitude of the experimental data.

3.2. Evaluation of the MD simulation results

Diffusion. In Fig. 6, the MSDs of water molecules are shown as a function of time during the 2 ns trajectories in each matrix. In these plots, MSDs are averaged over all water molecules and over all time origins. The general trend of the diffusion in SMA < PS < SBR is also observed for water.

In general, the long time limits of a trajectory are statistically unreliable, and the non-Einstein (anomalous) diffusion regime is observed at very short times [27]. As a result, in the intermediate region, the Einstein diffusion regime can be observed for relatively fast diffusing molecules and mobile matrices given that the slope of the log(MSD) vs. log(time) plot reaches unity. In Fig. 6, the

Table 8
Experimental (P_{exp}) and simulated (P_{sim}) permeability coefficients for SBR, PS and SMA (P is in (cm^3(STP) cm/cm^2 Pa s)

Gas type	Cells	$P_{exp} \times 10^{15}$ (SBR)	$P_{sim} \times 10^{15}$ (SBR)	$P_{exp} \times 10^{15}$ (PS)	$P_{sim} \times 10^{15}$ (PS)	$P_{exp} \times 10^{15}$ (SMA)	$P_{sim} \times 10^{15}$ (SMA)
He	Cell-1	1725[a]	5700	1400[b]	5900	–	2300
	Cell-2		7000		6800		3400
H_2	Cell-1	3080[a]	5800	1700[b]	4500	–	1300
	Cell-2		6700		5500		2000
Ne	Cell-1	–	1700	–	1600	–	360
	Cell-2		1800		1300		610
O_2	Cell-1	1275[a]	2500	200[b]	1400	45–50[c]	120
	Cell-2		1500		610		190
N_2	Cell-1	473[a]	480	59[b]	180	–	12
	Cell-2		250		88		25
CH_4	Cell-1	1580[a]	590	58.5[b]	130	–	9.7
	Cell-2		250		66		11
Ar	Cell-1	–	360 (1100)	–	100 (460)[d]	–	3.4 (26)[d]
	Cell-2		150 (660)		41 (200)[d]		7.7 (54)[d]
CO_2	Cell-1	9030[a]	710 (4500)	790[b]	140 (2000)[d]	36–54[c]	1.6 (56)[d]
	Cell-2		320 (2700)		26 (610)[d]		4.6 (160)[d]

[a] Ref. [33]. Butadiene/styrene (wt:wt parts%) 77:23.
[b] Ref. [36].
[c] Ref. [43]. Maleic anhydride/styrene (wt:wt parts%) 25:75.
[d] The values for the two gasses (Ar and CO_2) that are given in parentheses are computed by the σ_{Ar} and σ_{CO_2} of Table 2 which are shown in parentheses.

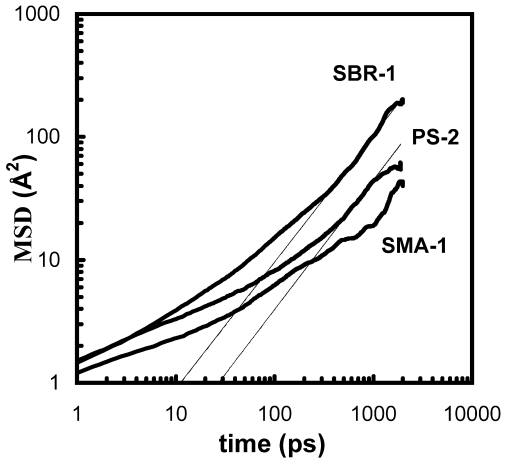

Fig. 6. Logarithmic plot of MSD vs. time for the diffusion of H_2O molecules in SBR-1, PS-2 and SMA-1 at 300 K. The thin lines with the slopes of $m = 1.05$ and 1.03 are drawn for PS-2 and SBR-1, respectively.

slope of log(MSD) vs log(t) curve increases approximately to unity after 500 and 350 ps for PS and SBR, respectively. The estimated diffusion coefficient of H_2O in PS is 0.52×10^{-6} cm^2/s, which is close to the experimental value of 0.14×10^{-6} cm^2/s [36] and it is 1.38×10^{-6} cm^2/s in SBR. On the other hand, since the Einstein diffusion regime is not reached during 2 ns of simulation time, the diffusion coefficient of H_2O in SMA is not calculated. However, we should note here that three-dimensional diffusion is not observed looking at the motion of individual water molecules. Following the path of individual penetrants in the 2 ns range, the principal moments of the radius of gyration tensor indicate one-dimensional diffusion rather than three, with one principal moment being much greater than the other two. Increasing the simulation time of PS to 4 ns indicated two-dimensional diffusion for most penetrants. In short, the diffusion coefficients reported above should be taken with caution, since they do not represent random walk of individual penetrants in three-dimensions, which may be a result of inadequate simulation time and aggregation of water molecules in PS and SBR.

The displacement of a specific gas molecule from its initial position at $t = 0$ to its final position at time t, i.e. $r(t) = \sqrt{|\boldsymbol{r}(t) - \boldsymbol{r}(0)|^2}$, can be plotted as a function of time to observe its diffusive behavior. Fig. 7(a)–(c) show the displacements of water molecules in SMA, PS and SBR, respectively. Three representative water molecules are chosen from each cell, named as H_2O-1, H_2O-2 and H_2O-3. For better visualization, the curves for H_2O-1 and H_2O-2 molecules have been shifted vertically by 11 and 6 Å in SMA, by 11 and 8 Å both in PS and SBR, respectively. In SMA, four out of eight molecules have not made any jumps, such as H_2O-3 molecule in Fig. 7(a). On the other hand, all molecules show at least one jump in PS and SBR. In the glassy matrices, there is an abundance of back-and-forth hopping between neighboring free volume sites, which does not contribute to the overall displacement of the molecules.

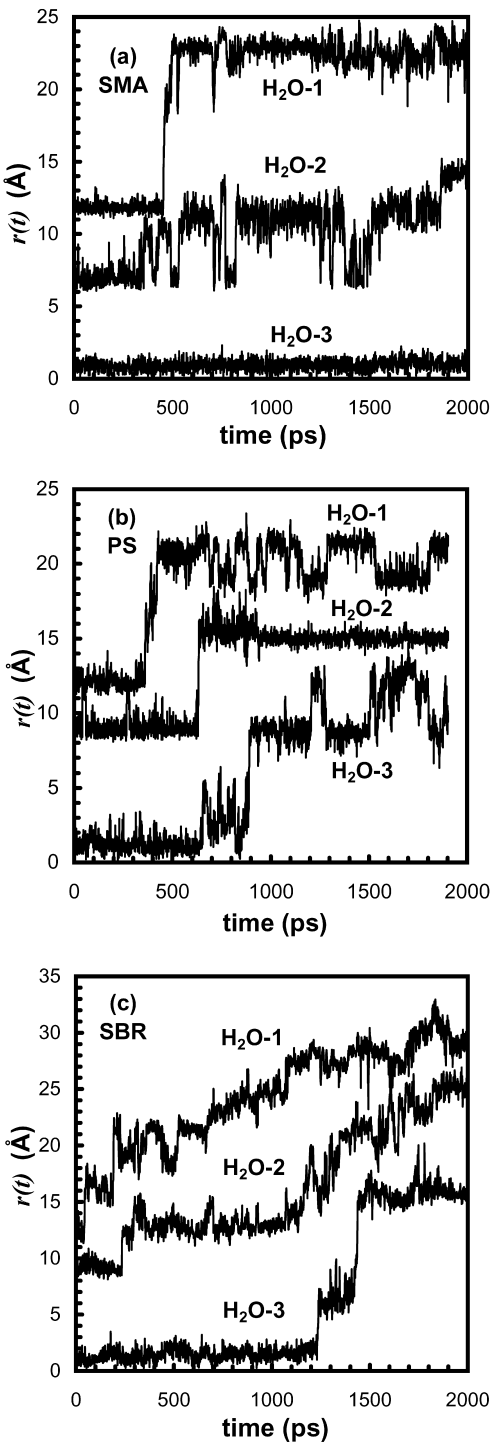

Fig. 7. Displacements of H_2O molecules from their original positions in (a) SMA, (b) PS, (c) SBR matrices. Three representative molecules are chosen from each cell. The displacements of the first and second molecules are shifted vertically, for clarity.

This phenomenon has been observed in previous work and attributed to the fact that the channels connecting neighboring free volume sites have much longer life times in frozen-glassy polymers than in rubbery polymers [28].

At the end of the 2 ns runs, three out of five water molecules (H_2O-1 and H_2O-2 are two of them) aggregated

in PS, whereas the water molecules in SBR aggregated in two separate groups, each containing two and three molecules. Aggregation of water molecules, which is also seen in previous MD simulations on polybenzoxazine matrix [20], does not take place in the polar SMA matrix during 2 ns. In fact, some of the aggregated water molecules also dissociate during the 2 ns trajectories, and dissociation is more frequent in SBR due to its mobility. We will look at this phenomenon in more detail in the section on pair correlation functions of water molecules.

Local relaxation of chains. The local dynamics of the matrices are studied using the rotational (orientational) time correlation function that is described by [48,49]

$$m(t) = \langle \mathbf{u}(t_0)\cdot\mathbf{u}(t_0 + t)\rangle \quad (7)$$

Here $\mathbf{u}(t)$ denotes a unit vector that characterizes the orientation of the main or side chain of the polymer at a given time, t. The ensemble average is evaluated on the basis of an ensemble of snapshots at various starting times, t_0.

The averages of the rotational time correlation functions for SMA, PS and SBR over their 2 ns dynamics in the presence of water molecules are computed. The local relaxation of the main chain is monitored by looking at the vectors that connect any $C(i)$ to $C(i+3)$ atoms in SMA and PS, which represent all the three-bond segments along the backbone. Also, the average relaxation of all the backbone bonds that connect $C(i)$ and $C(i+1)$ in SMA, PS and SBR is calculated. The relaxation of side chains are observed through the vectors that are fixed at the first and last carbon atoms of each c43–c3a–c3a–c3a sequence, which describes the average relaxation of the phenyl rings in each matrix. (see Fig. 1(a)).

In Fig. 8(a), there is no considerable structural relaxation of the main chain segments in the glassy systems, i.e. PS and SMA. However, a slight difference can still be observed in the local dynamics of these matrices in the short time scales of 50–100 ps. The initial decay in the orientational autocorrelation of the main chain vectors is faster in PS compared to SMA, even though both functions level off to almost the same value.

In the case of side chain relaxations, the orientational autocorrelation of the phenyl rings exhibits a relatively faster and more appreciable decrease in PS than in SMA (lower two curves in Fig. 8(a)). Thus, the differences in the local mobility of the two glassy matrices may (at least partially) explain the slower diffusion of water molecules in SMA compared to PS. Because the fast hopping events of the penetrant, which occur in several ps, should be sensitive to these differences in local dynamics in the 50–100 ps time scale.

In comparison to the glassy matrices, rubbery SBR exhibits much faster and cooperative relaxations of the main and side chain vectors, as shown in Fig. 8(b). The long-time relaxation behavior of PS and SMA over the 1000 ps range is indistinguishable, so only PS is plotted

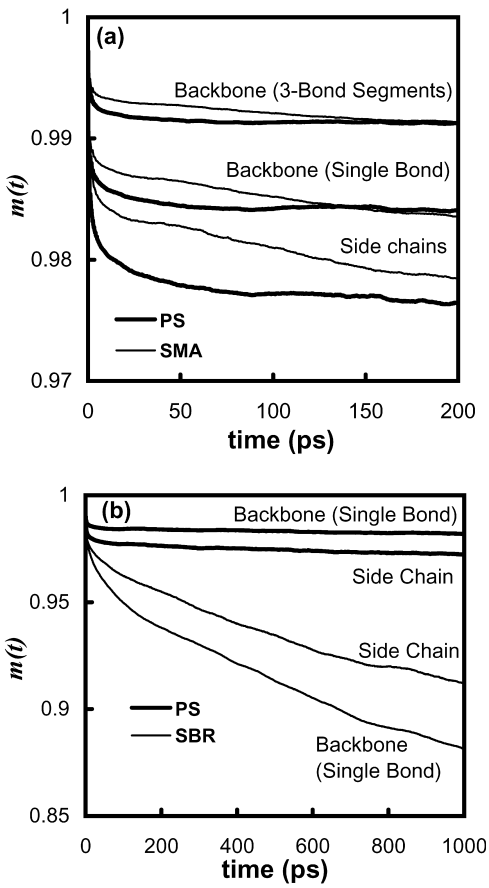

Fig. 8. The rotational time correlation function during NVT dynamics for the main and side chain vectors of (a) PS, SMA (b) PS, SBR.

here for comparison to the rubbery matrix. Moreover, the curves for SBR do not level off to constant values (in the range of 0.98–0.99) as in the case of glassy polymers, but show continual decay. Thus, the high mobility of the rubbery matrix is a reason for the faster diffusion observed.

Structure of the matrices. In Fig. 9(a), the simulated X-ray scattering patterns are compared for different amorphous cells, as a function of the scattering vector q. For PS, the experimental peaks located at $q = 0.75$, 1.4 and 3.0 Å^{-1} are detected within 0.1 Å^{-1} accuracy in our simulations (PS-2 shown) [50,51]. Moreover, the relative intensities of these three peaks fall into the ranges presented in previous work [32]. The first two peaks observed at the lower q region are sensitive to intermolecular packing and structural relaxations [32,50,51]. Similar peaks are observed in SMA structures, with the location of the lowest q peak being appreciably different between SMA-1 ($q \approx 0.5$ Å^{-1}) and SMA-2 ($q \approx 0.8$ Å^{-1}, not shown), which also have quite different solubility parameters (Table 4).

The COMPASS forcefield includes a Lennard–Jones 9–6 potential for van der Waals type interactions and a Coulombic term for the electrostatic interactions. Partial charges are assigned to the H and C atoms on the backbone and the phenyl ring in a similar fashion to the forcefield used

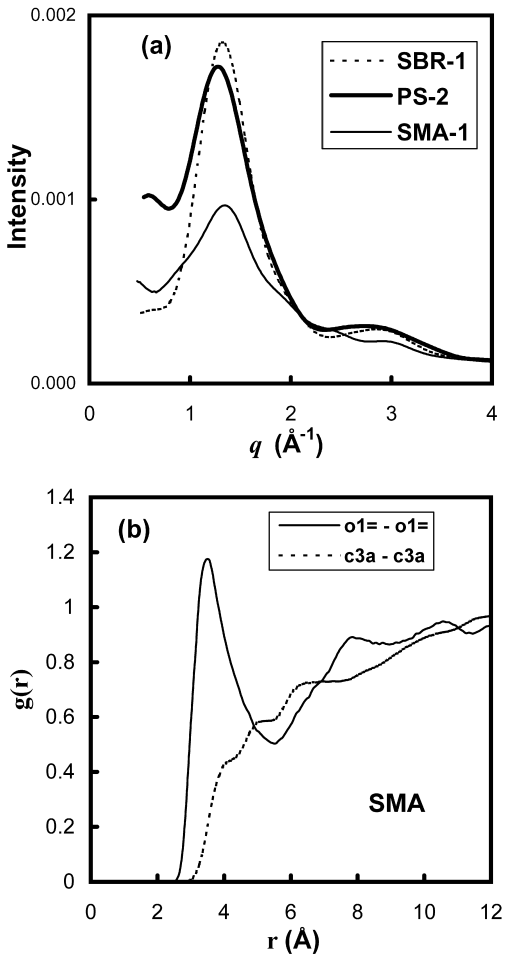

Fig. 9. (a) X-ray scattering patterns for PS-2, SMA-1, SBR-1 as a function of scattering vector q ($Å^{-1}$), (b) the intermolecular pair correlation function, $g(r)$, of carbon (c3a) atoms and oxygen (o1 =) atoms of SMA.

by Rapold and Suter, which are stated to be important for ring–ring interactions and intermolecular packing in PS [52]. We should also note that the amorphous cell method [37] used in this work is known to lead to deviations from rotational isomeric state (RIS) models [38,53] for glassy polymers with bulky side groups, such as PS [54]. Even though the PolyPack algorithm [55], which seems more suitable for the packing of PS, is not used here, still the predicted diffusion coefficients are close to experimental results, i.e. not affected by probable deviations from *theta* state or RIS conformations.

Fig. 9(b) compares the pair correlation function, $g(r)$, of the two repeat units of SMA. The dashed line gives the intermolecular $g(r)$ for carbon (c3a) atoms of the phenyl ring. This form is very similar to what is observed in SBR and PS for the aromatic carbons. In the same figure, the solid line gives intermolecular $g(r)$ for the carbonyl oxygen atoms (o1=) on the maleic anhydride repeat unit. Here, the peak at around 3.5 Å indicates the clustering of maleic anhydride repeat units. Investigation of the local SMA structure around specific water molecules does not show any clear difference among the water molecules that exhibit and do not exhibit jumps, such as respective H_2O-1 and H_2O-3 in Fig. 7(a).

Pair correlation functions of water molecules. The interactions between H_2O molecules and some selected atoms of polymer chains are shown in Fig. 10(a)–(c). In all following calculations, the interaction site for the water molecule is chosen as the oxygen atom (o2*). In Fig. 10(a), the pair correlation function, $g(r)$, between water molecules and the o1= potential type assigned oxygen atoms of SMA shows a sharp peak at a distance of ≈2.85 Å, which is the sum of the hard sphere radii of two oxygen atoms. This indicates the occurrence of the hydrogen bonding between water molecules and carbonyl oxygens of SMA. The pair correlation function between the o2b potential type assigned oxygen atoms and water molecules also shows a peak at the hydrogen bonding distance of 3.15 Å and a second peak at 4.95 Å, possibly resulting from the water molecules that form H-bonds with the carbonyl oxygens of SMA. Other than the distributions that indicate the H-bonding capacity of SMA, Fig. 10(b) shows the interactions between water molecules and the carbon atoms of the phenyl side chains (c3a) in the different matrices. The peaks located at around 3.6 Å indicate the exposure of phenyl side chains to the water molecules residing in the free volumes. The probability of these specific interactions with water molecules, given by the height of the peaks, can be compared in different matrices as SBR > PS > SMA.

The interactions among different water molecules (o2* atoms) residing in the same cell are displayed in Fig. 10(c) for PS, SMA and SBR. The high peaks located at about 2.85 Å indicate that there is appreciable self-aggregation among water molecules in the nonpolar systems: PS and SBR. In comparison, the excessive hydrogen bonding among the maleic anhydride residues and water molecules and slower penetrant diffusion in SMA possibly hinders the self-aggregation of water molecules, as a result of which a relatively small peak is observed around 2.85 Å.

4. Concluding remarks

Transition state approach is used to calculate the diffusion coefficients (D) and the solubility values (S) of simple gases in SMA, PS and SBR matrices, and also predict the permeability coefficient (P) as the product of D and S. As a result, gas transport parameters in these matrices are estimated with reasonable accuracy, i.e. within less than an order of magnitude of the experimental results. The permeability of these matrices to simple gases decreases in the following order: P(SBR) > P(PS) > P(SMA). The diffusion coefficients, which decrease in the same order, are more dominant in determining the permeability coefficients compared to solubility coefficients of the same gases, which follow the reverse order as: S(SBR) < S(PS) < S(SMA).

Our TSA results on simple gases are in conformity with

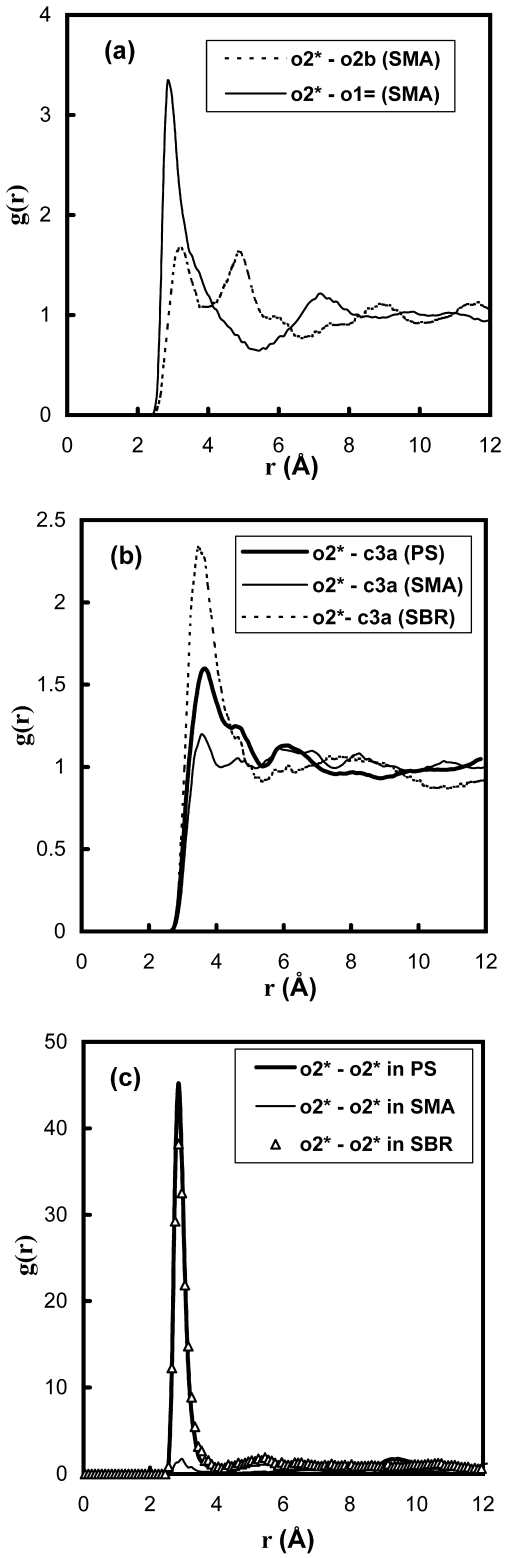

Fig. 10. The intermolecular pair correlation function of the oxygen atoms of water molecules (a) with oxygen atoms of SMA, (b) with phenyl ring carbon atoms (c3a) of PS, SMA, SBR, and (c) among themselves.

the correlations that relate the diffusion coefficient to the effective penetrant diameter and the solubility values to the effective Lennard–Jones parameter of the gases [45]. Inspection of the correlation coefficients for diffusion in different matrices (see Eq. (4) and Table 6) indicate that K_2 (SMA: glassy, polar) $>$ K_2 (PS: glassy, nonpolar) $>$ K_2 (SBR: rubbery), in conformity with a previous compilation of experimental results [45]. In general, the difference between the diffusion coefficients in the three matrices becomes more pronounced as the effective penetrant diameter increases.

Local mobility of the polymer chains, given by the smear factors in TSA, seems to be the dominant factor that determines the diffusion coefficients in these matrices, especially in the glassy ones. In contrast, the free volume distribution of the matrices affects the solubility values, but not the diffusion coefficients, in agreement with previous work on glassy polypropylene [6].

MD simulations on water diffusion indicate the same trend as TSA results on simple gases, i.e. SBR $>$ PS $>$ SMA. We could not estimate a diffusion coefficient for SMA, because the Einstein diffusion regime is not reached during the 2 ns trajectory. The orientational autocorrelation functions of the backbone bonds and the side chains (phenyl rings) show substantial relaxation in the rubbery matrix compared to the glassy ones, as expected. And the local mobility of PS is higher compared to SMA. Inspection of the displacement paths of specific water molecules shows that the back-and-forth hops between neighboring free volume sites are abundant in glassy matrices due to long-living channels, which has been previously indicated by Hofmann et al. [28]. In PS and SBR, we detect aggregation of water molecules in groups of two or three, and also the dissociation of aggregated molecules during the trajectories. In SMA, water molecules form hydrogen bonds with the maleic anhydride residues.

In summary, our work provides estimates of D and S for SMA, which has not been reported before at least to our knowledge. Moreover, the equilibrium and dynamics properties of the two copolymers, SBR and SMA, are characterized on a microscopic scale in relationship to the transport of gases in these matrices.

Acknowledgements

This work has been supported by the Bogazici University B.A.P. (01HA501), DPT Project (01K120280), ARCELIK A.S, and the Turkish Academy of Sciences in the framework of the Young Scientist Award Program (PD-TUBA-GEBIP/2002-1-9). The authors thank Turgut and Nihan Nugay for their suggestion of the SMA matrix.

References

[1] Comyn J. Polymer permeability, 2nd ed. London: Chapman & Hall; 1994.

[2] Vieth WR. Diffusion in and through polymers. Munich: Hanser; 1991.
[3] Theodorou DN. In: Neogi P, editor. Diffusion in polymers. New York: Marcel Dekker Inc; 1996. p. 67.
[4] Müller-Plathe F. J Chem Phys 1991;94:3192.
[5] Müller-Plathe F. J Chem Phys 1992;96:3200.
[6] Cuthbert TR, Wagner NJ, Paulaitis ME, Murgia G, D'Aguanno B. Macromolecules 1999;32:5017.
[7] Boyd RH, Pant PVK. Macromolecules 1991;24:6325.
[8] Müller-Plathe F, Rogers SC, van Gunsteren WF. Macromolecules 1992;25:6722.
[9] Pant PVK, Boyd RH. Macromolecules 1993;26:679.
[10] Müller-Plathe F, Rogers SC, van Gunsteren WF. J Chem Phys 1993; 98:9895.
[11] Tamai Y, Tanaka H, Nakanishi K. Macromolecules 1994;27:4498.
[12] Sok RM, Berendsen HJC, van Gunsteren WF. J Chem Phys 1992;96: 4699.
[13] Charati SG, Stern SA. Macromolecules 1998;31:5529.
[14] Gee RH, Boyd RH. Polymer 1995;36:1435.
[15] Han J, Boyd RH. Polymer 1996;37:1797.
[16] Hofman D, Ulbrich J, Fritsch D, Paul D. Polymer 1996;37:4773.
[17] Zhang R, Mattice WL. J Membr Sci 1995;108:15.
[18] Müller-Plathe F. J Membr Sci 1998;141:147.
[19] Tamai Y, Tanaka H. Fluid Phase Equilibria 1998;144:441.
[20] Kim WK, Mattice WL. Macromolecules 1998;31:9337.
[21] Fried JR, Sadat-Akhavi M, Mark JE. J Membr Sci 1998;149:115.
[22] Fried JR, Goyal DK. J Polym Sci: Part B: Polym Phys 1998;36:519.
[23] Fried JR, Ren P. Comput Theor Polym Sci 2000;10:447.
[24] Tocci E, Hofman D, Paul D, Russo N, Drioli E. Polymer 2001;42:521.
[25] Gusev AA, Arizzi S, Suter UW, Moll DJ. J Chem Phys 1993;99:2221.
[26] Gusev AA, Arizzi S, Suter UW. J Chem Phys 1993;99:2228.
[27] Gusev AA, Müller-Plathe F, van Gunsteren WF, Suter UW. Adv Polym Sci 1994;116:207.
[28] Hofman D, Fritz L, Ulbrich J, Paul D. Comput Theor Polym Sci 2000; 10:419.
[29] Lopez-Gonzales M, Saiz E, Guzman J, Riande E. J Chem Phys 2001; 115:6728.
[30] Cuthbert TR, Wagner NJ, Paulaitis ME. Macromolecules 1997;30: 3058.
[31] Khare R, Paulaitis ME. Macromolecules 1995;28:4495.
[32] Kotelyanskii M, Wagner NJ, Paulaitis ME. Macromolecules 1996;29: 8497.
[33] Roff WJ, Scott JR, Pacitti J. Fibres, films, plastics and rubbers, 1st ed. A handbook of common polymers, London: Butterworths; 1971.
[34] Accelrys Inc, San Diego, CA, USA (Insight II 4.0.0 P+, POLYMERIZER, DISCOVER, AMORPHOUS_CELL, BUILDER and RIS Modules version 2001.11).
[35] COMPASS—Condensed Phase Optimized Molecular Potentials for Atomistic Simulation Studies. Distributed by Accelrys Inc.; 1999.
[36] Brandrup J, Immergut EH, Grulke EA. Polymer handbook, 4th ed. Canada: Wiley; 1999.
[37] Theodorou DN, Suter UW. Macromolecules 1985;18:1467.
[38] Flory PJ. Statistical mechanics of chain molecules. New York: Wiley; 1969.
[39] Andersen HC. J Chem Phys 1980;72:2384.
[40] Berendsen HJC, Postma JPM, van Gunsteren WF, DiNola A, Haak JR. J Chem Phys 1984;81:3684.
[41] GSNET&GSDIF Macros, Distributed by Accelrys Inc., San Diego, CA, USA.
[42] Crank J, Park GS. Diffusion in polymers, 2nd ed. New York: Academic Press; 1975.
[43] Mark HF, Bikales NM, Overberger CG, Menges G. Encyclopedia of polymer science and engineering. Canada: Wiley; 1989.
[44] Van Krevelen DW. Properties of polymers. Netherlands: Elsevier Science; 1990. Chapter 18.
[45] Teplyakov V, Meares P. Gas Separation Purification 1990;4:66.
[46] Toi K, Morel G, Paul DR. J Appl Polym Sci 1982;27:2997.
[47] Vieth RW, Tam PM, Michaels AS. J Colloid Interface Sci 1966;22: 360.
[48] Allen MP, Tildesley DJ. Computer simulation of liquids. Oxford: Clarendon Press; 1989.
[49] Bahar I, Badur B, Doruker P. J Chem Phys 1993;99:2235.
[50] Mitchell GR, Windle AH. Polymer 1984;25:906.
[51] Song HH, Roe RJ. Macromolecules 1987;20:2723.
[52] Rapold RF, Suter UW. Macromol Theory Simul 1994;3:1.
[53] Mattice WL, Suter UW. Conformational theory of large molecules, the rotational isomeric state model in macromolecular systems. New York: Wiley; 1994.
[54] Robyr P, Muller M, Suter UW. Macromolecules 1999;32:8681.
[55] Muller M, Nievergelt J, Santos S, Suter UW. J Chem Phys 2001;114: 9764.